Optics Letters

Light guiding above the light line in arrays of dielectric nanospheres

Evgeny N. Bulgakov[1,2] and Dmitrii N. Maksimov[1,*]

[1]Kirensky Institute of Physics, 660036 Krasnoyarsk, Russia
[2]Siberian State Aerospace University, 660014 Krasnoyarsk, Russia
*Corresponding author: mdn@tnp.krasn.ru

Received 12 May 2016; revised 26 July 2016; accepted 27 July 2016; posted 28 July 2016 (Doc. ID 265006); published 15 August 2016

We consider light propagation above the light line in arrays of spherical dielectric nanoparticles. It is demonstrated numerically that quasi-bound leaky modes of the array can propagate both stationary waves and light pulses to a distance of 60 wavelengths at the frequencies close to the bound states in the radiation continuum. A semi-analytical estimate for decay rates of the guided waves is found to match the numerical data to a good accuracy.

OCIS codes: (050.6624) Subwavelength structures; (250.5530) Pulse propagation and temporal solitons.

http://dx.doi.org/10.1364/OL.41.003888

The progress in subwavelength optics opens unprecedented opportunities for manipulating light on the nanoscale [1–3]. Among those is the fabrication of subwavelength waveguides which may serve as the key components for future integrated optics [4–8]. Since the seminal Letter by Quinten *et al.* [4], one of the mainstream ideas in the design of subwavelength waveguides has been the implementation of various assemblies of plasmonic nanoparticles such as those considered in [6,9–15], to name a few relevant references from the vast literature on the subject. Seemingly less attention, though, has been paid to the arrays of dielectric nanoparticles [16–21], although all-dielectric nanooptics [22] could be potentially advantageous against nanoplasmonics due to, for instance, the opportunity to control the frequencies of electric and magnetic Mie resonances by changing the geometry of high-index nanoparticles and the absence of free carriers, resulting in a high Q-factor. Arguably, the arrays of dielectric nanoparticles provide one of the most promising subwavelength setups for efficient light guiding [20,21,23], as well as more intricate effects such as resonant transmission of light [24] and optical nanoantennas [25].

So far, the major theoretical tool for analyzing the infinite arrays of spherical dielectric nanoparticles has been the coupled dipole approximation [26–28]. In this approximation, guided waves in arrays of magnetodielectric spheres were first considered by Shore and Yaghjian [29,30] who derived the dispersion relation and computed the dispersion curves for dipolar waves. Recently, a more tractable form of the dispersion equations was presented by the same authors [31] with the use of the polilogarithmic functions. The dipolar waves in arrays of Si dielectric nanospheres were thoroughly analyzed in [23]. It was shown that only two of the lowest guided modes could be fairly described by the dipole approximation which breaks down as the frequency approaches the first quadruple Mie resonance. This limits the application of the dipolar dispersion diagrams to realistic waveguides assembled of dielectric nanoparticles. As an alternative to the dipole approximation, a "semiclassical" approach based on the coupling of the whispering gallery modes of individual spheres could be employed to recover the array band structure [32,33] if the wavelength is much smaller than the diameter of the spheres. The general case, however, requires a full-wave Mie scattering approach to account for all possible multipole resonances [17] involving a very complicated multiscattering picture which mathematically manifests itself in infinite multipole sums. Luckily, such an approach was recently developed by Linton, Zalipaev, and Thompson who managed to obtain a multipole dispersion relation in a closed form suitable for numerical computations [34]. The above approach was used for analyzing the spectra of dielectric arrays above the line of light in [35]. It was demonstrated that under variation of some parameters such as the radius of the spheres, the leaky modes dominating the spectrum can acquire an infinite lifetime. In other words, the array can support bound states in the radiation continuum (BSCs) [36–40]. In this Letter, we will address the ability of the BSCs to propagate light along the array, primarily motivated by finding new opportunities for designing subwavelength waveguides.

Let us first obtain the dispersion diagram of an array of dielectric nanoparticles. The dispersion curves are computed by solving the dispersion equation $f_{d,m}(k,\beta) = 0$, where k is the vacuum wave number $k = \omega/c$, and β is the Bloch wave number, while the subscripts d, m designate either dipole [23,31] or multipole [34] dispersion relations. For brevity, we do not present the exact dispersion relations $f_{d,m}(k,\beta) = 0$. A mathematically inquisitive reader is referred to the above cited Letters to examine the rather cumbersome expressions for $f_{d,m}(k,\beta)$. Here we assume that the array consists of spherical nanoparticles of radius R with a dielectric constant $\epsilon = 15$ (Si) in vacuum. The centers of the nanoparticles are separated by distance a. It is worth mentioning that at a given dielectric

constant, the dispersion is only dependent on a single dimensionless quantity R/a. This allowed the scaling of the model for a microwave experiment [23]. There are three types of dipolar solutions [23], namely, longitudinal magnetic (LM), longitudinal electric (LE), and transverse electromagnetic (TEM) waves. In Fig. 1, we plot the lowest frequency modes of each type in comparison with the multipole solution [34]. In all cases, if the $k-\beta$ curve is above the light line $k=\beta$, the vacuum wave number becomes complex valued. The imaginary part of k is linked to the mode lifetime through the following formula:

$$\tau = -[c\Im(k)]^{-1}. \quad (1)$$

Two approaches are possible for the description of the leaky modes: complex frequency ω [41,42] or complex Bloch number β [23,43]. In the latter case, the inverse of the imaginary part of β is the penetration depth into the array $L_\tau = [\Im(\beta)]^{-1}$. The quantities τ and L_τ are, in fact, proportional:

$$L_\tau = v\tau, \quad (2)$$

where v is the group velocity $v = d\Re(\omega)/d\beta$. Here, we do not present the imaginary part of β, mentioning in passing that the penetration depths for dipolar waves were analyzed in [23,43]. Importantly, the numerical data available so far [23,35,43] indicate that all dipolar leaky modes are relatively short-lived; in particular, no dipolar BSCs were found in [35]. In compliance with [23], Fig. 1 demonstrates that only two of the lowest eigenmodes are fairly described by the dipole approximation. Thus, for obtaining valid results for guided modes at $ka/\pi \geq 1$, one has to resort to the full-wave formalism of [34].

Now, let us consider the multipolar quasi-guided modes within the first radiation continuum [35]. The dispersion curves for a leaky mode for two different ratios R/a are plotted in Fig. 2(a). One can see that, in contrast to the dipolar waves in

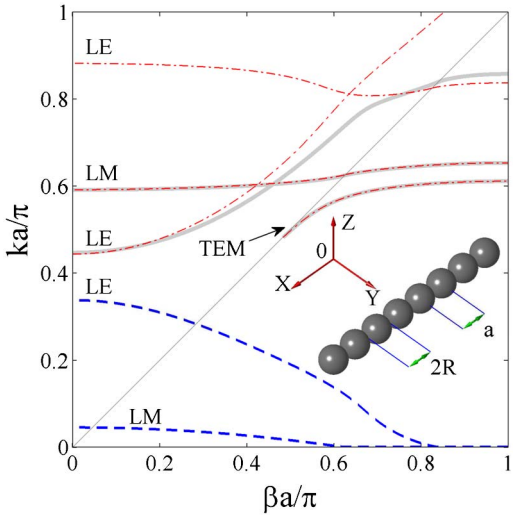

Fig. 1. Dispersion diagram of an infinite array of dielectric nanospheres of radius R with dielectric constant $\epsilon = 15$, $R/a = 0.4$. The array centerline is aligned with the x-axis, as shown in the southeast corner of the plot. The real parts of the solutions are shown by dashed-dotted red lines. The thick gray lines are the real parts of the full-wave solutions; the negative imaginary parts $-\Im(k)$ of the full-wave solutions are shown by the blue dashed lines. The thin gray line is the light line.

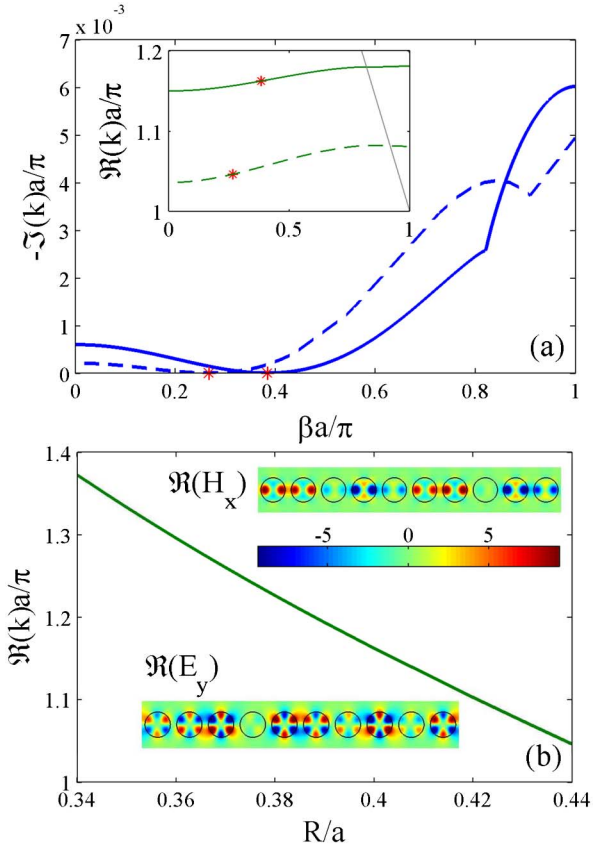

Fig. 2. (a) Quasi-guided modes above the light line; $R/a = 0.4$, solid line; $R/a = 0.44$, dashed line; $\epsilon = 15$. Imaginary part of k, the main plot; real part, the inset. The positions of the BSCs are shown by the red stars. The imaginary parts are non-smooth, as the real parts cross the boundary of the second radiation continuum $ka = 2\pi - \beta a$ shown by thin gray line. (b) Bloch BSC $\beta \neq 0$ vacuum wave number k versus R/a, $\epsilon = 15$. The insets show the real parts of the y-component of the electric vector E_y and the x-component of the magnetic vector H_x in the $x0y$-plane for the BSC at $R/a = 0.4$.

Fig. 1, now the solutions could be long-lived with the lifetime Eq. (1) growing up to infinity at the BSC points. It should be pointed out that for both R/a of all leaky modes of the array we plot only one which has a Bloch BSC point $\Im(k) = 0$ at $\beta \neq 0$. As shown in Fig. 2(b) the BSC exists in a wide range of parameter R/a. The magnetic and electric vectors could be found in terms of Mie coefficients a_n^m, b_n^m. For instance, outside the spheres one has for the electric vector $\mathbf{E}(\mathbf{r})$ [34]:

$$\mathbf{E}(\mathbf{r}) = \sum_{j=-\infty}^{\infty} e^{iaj\beta} \sum_{n=m^*}^{\infty} [a_n^m \mathbf{M}_n^m(\mathbf{r} - \mathbf{r}_j) + b_n^m \mathbf{N}_n^m(\mathbf{r} - \mathbf{r}_j)], \quad (3)$$

where j the number of the particle in the array, m—azimuthal number; $m^* = \max(1, m)$; and $\mathbf{N}_n^m(\mathbf{r})$, $\mathbf{M}_n^m(\mathbf{r})$ are spherical vector harmonics [44]. Only $m = 0$ Bloch BSCs were found in [35]. Our numerics indicate that for BSCs in Fig. 2 the dominating term in the expansions (3) corresponds to coefficient a_3^0. In the insets in Fig. 2(b), we plot the components of the electric and magnetic vectors of the BSC solution. One can see that the electromagnetic field is localized in the vicinity of the array. To run the numerical simulations, a finite number

Table 1. BSC Vacuum Wave Vector and Bloch Number for Different Numbers of Multipoles M, $R/a = 0.4$, $\epsilon = 15$

M	4	6	7	8
ka/π	1.16202626	1.16200043	1.16199989	1.16199928
$\beta a/\pi$	0.38409318	0.38395427	0.38395035	0.38394978

of spherical harmonics M was used instead of the infinite sum in Eq. (3). According to [34], the above described approach converges exponentially with M. In Table 1, we illustrate the convergence for the data from Fig. 2(a); one can see that $M = 7$ is already sufficient for the relative error of order 10^{-5}.

The amplitude of a wave propagating along the array attenuates exponentially according to a simple formula:

$$F(x) = e^{-x/L_\epsilon}, \tag{4}$$

where $x = ja$ is the distance. In the vicinity of a BSC, the $\omega - \beta$ dependence could be approximated as

$$\omega - \omega_0 = v_0(\beta - \beta_0) + \mathcal{O}[(\beta - \beta_0)^2], \tag{5}$$

where ω_0, β_0, v_0 are the BSC eigenfrequencies, Bloch number, and group velocity, correspondingly:

$$-\Im\{k\} = \alpha(\beta - \beta_0)^2 + \mathcal{O}[(\beta - \beta_0)^3]. \tag{6}$$

Combining Eqs. (1), (2), and (4)–(6) one obtains in the vicinity of a BSC:

$$F(x) = \exp\left[-\frac{\alpha x c}{v_0^3}(\omega - \omega_0)^2\right]. \tag{7}$$

Thus, for the width of the transparency window in the frequency domain, we have

$$\Delta(x) = \sqrt{\frac{v_0^3}{\alpha c}}\frac{1}{\sqrt{x}}, \tag{8}$$

with α and v_0 extracted from the data in Fig. 2 by a polynomial fit. Nevertheless, care is needed in applying Eq. (7) as the frequency may fall out of the range, where the dispersion is well approximated by the leading terms in Eqs. (5) and (6).

Using a full-wave multiscattering method [17], we simulated wave propagation in a finite array of 400 nanoparticles. In our numerical experiment, a linearly polarized Gaussian beam [45] with the Rayleigh range $z_0 = 5a$ was focused on the first nanoparticle in the array. The wave vector of the beam was directed along the y-axis perpendicular to the array (see Fig. 1), and the magnetic vector aligned with the array axis. In Fig. 3(a), we plot the leading Mie coefficient a_3^0 for the last nanoparticle in the array. The result shows a pronounced resonant behavior due to the formation of standing waves as a consequence of the finiteness of the array. The distance between the resonances $\Delta\omega$ could be assessed as $\Delta\omega \approx \pi v_0/(aN)$, where N is the number of particles in the array. The resonant features could be averaged out by integration over small frequency intervals larger than $\Delta\omega$. The result is shown in Fig. 3(a) in comparison with Eq. (7). One can see that Eq. (7) matches the numerical data to a good accuracy. The finiteness of the chain also results in additional attenuation due to the radiative losses at the ends of the array. A detailed study of the effect was undertaken in [17], where it was shown that the Q factor of the finite arrays of high-index nanoparticle scales was CN^3 with $0.1 < C < 10$ which makes such

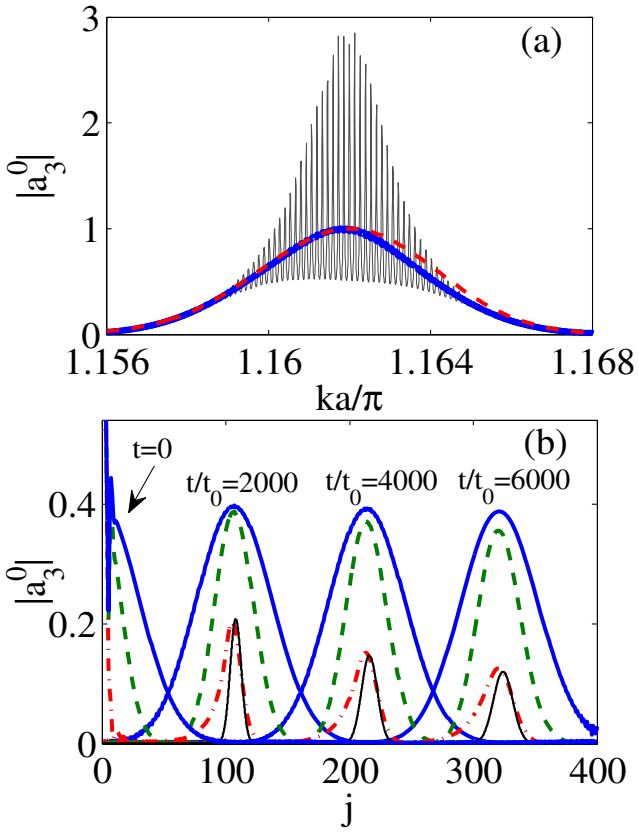

Fig. 3. Light propagation in the array of 400 nanoparticles $\epsilon = 15$, $R/a = 0.4$, and $v_0 = 0.054c$, $\alpha = 0.005a$. (a) Absolute value of the leading coefficient a_3^0 versus wave number k of the stationary wave injected into the array. The averaged data are plotted by a thick blue line against the analytical result Eq. (7), shown by the dashed red line. (b) Absolute value of the leading coefficient a_3^0 versus the particle number j for a light pulse with $k_0 = \pi 1.162/a$, $t_0 = a/c$. The pulse widths $\sigma_\omega = 0.0025/t_0$, blue solid; $\omega = 0.005/t_0$, green dashed; $\omega = 0.025/t_0$, red dashed-dotted lines. Thin black line shows the analytical result Eq. (9) for the pulse with $\sigma_\omega = 0.025/t_0$.

radiative losses negligible for $N = 400$. The discrepancy in Fig. 3 is due to the higher-order terms in Eqs. (5) and (6).

Finally, the pulse propagation along the array was considered in the above setup with a continuous superposition of Gaussian beams forming a Gaussian light pulse of width σ_ω in the frequency domain. The central wave number of the pulse was adjusted to the BSC wave number $k_0 = \pi 1.162/a$. At $t = 0$ a light pulse was injected into the left end of the array. In Fig. 3(b), we plot four snapshots of the leading Mie coefficient a_3^0 against the distance along the array for three different initial pulse widths σ_ω. One can clearly see in Fig. 3(b) that the pulse propagating along the array tends to spread as the harmonics distant in the ω-space from the BSC frequency decay into the continuum. The pulse profile $f(x, t)$ could be found by Fourier-transforming the initial Gaussian pulse to the real space:

$$f(x, t) = \frac{1}{\sigma(t)} e^{-\frac{(x - v_0 t)^2}{\sigma^2(t)}} e^{i(\beta_0 x - \omega_0 t)}, \tag{9}$$

with

$$\sigma^2(t) = 4a^2\left[\left(\frac{v_0}{a\sigma_\omega}\right)^2 + \frac{c\alpha}{a^2}t\right]. \quad (10)$$

Analyzing Eq. (10) for a given distance $L = v_0 t$, one can identify two possible regimes for the pulse propagation. In the "overdamped" regime, the second term dominates on the left-hand side of Eq. (10), resulting in a noticeable spreading of the pulse in the real space. If, however, the first term dominates, the pulse retains its profile during the propagation time [$\sigma_\omega = 0.0025/t_0$ in Fig. 3(b)]. One finds from Eq. (10) that the pulse doubles its width after traveling to the distance:

$$L = \frac{3a^2}{\alpha}\left(\frac{v_0}{c}\right)^3\left(\frac{c}{a\sigma_\omega}\right)^2. \quad (11)$$

So far, we neglected the material losses due to the imaginary part of the dielectric constant. Particularly, in silicon, the material losses vary significantly in the optical range [46]. We ran a numerical test at 725 nm with $\Im(\epsilon) = 0.0075$ to find that the propagation distance $L \approx 100a$, $a = 421$ nm, so the light can travel to approximately 60 wavelengths. It should be pointed out that in the near infrared $\lambda \approx 1000$ nm the losses can be tens of times less, allowing propagation to hundreds of wavelengths [23], as shown in Fig. 3.

We demonstrated the effect of light guiding above the light line in arrays of dielectric nanospheres. For the guiding of light, we employed leaky modes residing in the radiation continuum. It was found that long-lived leaky modes are associated with bound states in the continuum which are supported by the arrays in a broad range of parameters. The reported mutiplolar solutions, though still in the subwavelength range, have a higher R/λ ratio than the dipolar solutions in [23]. This, on the other hand, relaxes the condition $\lambda > 2a$ for guided waves in arrays and gratings [17]. Besides the fundamental aspects, the benefits of employing leaky modes could be the opportunity to guide light harvested from free waves propagating in the ambient medium [35,38], as well as a potential capacity to guide multiple frequencies of light, both below and above the radiation continuum in the same subwavelength structure. Finally, some remarks are due on the mechanism of the BSC formation. It was recently demonstrated in [47] that Bloch BSCs in photonic crystal slabs are vortex centers in the polarization directions of far-field radiation. We speculate that the same topological mechanism applies in the case of arrays of dielectric nanospheres. This result will be reported in more detail elsewhere.

Funding. Russian Foundation for Basic Research (RFBR) (16-02-00314).

Acknowledgment. The authors acknowledge discussions with A. F. Sadreev, A. S. Aleksandrovsky, and A. M. Vyunishev.

REFERENCES

1. W. L. Barnes, A. Dereux, and T. W. Ebbesen, Nature **424**, 824 (2003).
2. L. Novotny and B. Hecht, *Principles of Nano-Optics* (Cambridge University, 2012).
3. J.-H. Park, C. Park, H. Yu, J. Park, S. Han, J. Shin, S. H. Ko, K. T. Nam, Y.-H. Cho, and Y. Park, Nat. Photonics **7**, 454 (2013).
4. M. Quinten, A. Leitner, J. R. Krenn, and F. R. Aussenegg, Opt. Lett. **23**, 1331 (1998).
5. M. Law, Science **305**, 1269 (2004).
6. D. F. Pile and D. K. Gramotnev, Opt. Lett. **30**, 1186 (2005).
7. M. Skorobogatiy, *Nanostructured and Subwavelength Waveguides: Fundamentals and Applications* (Wiley, 2012).
8. X. Guo, Y. Ying, and L. Tong, Acc. Chem. Res. **47**, 656 (2014).
9. M. L. Brongersma, J. W. Hartman, and H. A. Atwater, Phys. Rev. B **62**, R16356 (2000).
10. S. A. Maier, P. G. Kik, and H. A. Atwater, Phys. Rev. B **67**, 205402 (2003).
11. W. H. Weber and G. W. Ford, Phys. Rev. B **70**, 125429 (2004).
12. A. Alù and N. Engheta, Phys. Rev. B **74**, 205436 (2006).
13. X.-X. Liu and A. Alù, Phys. Rev. B **82**, 144305 (2010).
14. F. Rüjting, Phys. Rev. B **83**, 115447 (2011).
15. I. L. Rasskazov, S. V. Karpov, and V. A. Markel, Opt. Lett. **38**, 4743 (2013).
16. A. L. Burin, H. Cao, G. C. Schatz, and M. A. Ratner, J. Opt. Soc. Am. B **21**, 121 (2004).
17. G. S. Blaustein, M. I. Gozman, O. Samoylova, I. Y. Polishchuk, and A. L. Burin, Opt. Express **15**, 17380 (2007).
18. M. Gozman, I. Polishchuk, and A. Burin, Phys. Lett. A **372**, 5250 (2008).
19. R. Zhao, T. Zhai, Z. Wang, and D. Liu, J. Lightwave Technol. **27**, 4544 (2009).
20. J. Du, S. Liu, Z. Lin, J. Zi, and S. T. Chui, Phys. Rev. A **79**, 205436 (2009).
21. J. Du, S. Liu, Z. Lin, J. Zi, and S. T. Chui, Phys. Rev. A **83**, 035803 (2011).
22. R. S. Savelev, S. V. Makarov, A. E. Krasnok, and P. A. Belov, Opt. Spectrosc. **119**, 551 (2015).
23. R. S. Savelev, A. P. Slobozhanyuk, A. E. Miroshnichenko, Y. S. Kivshar, and P. A. Belov, Phys. Rev. B **89**, 035435 (2014).
24. R. S. Savelev, D. S. Filonov, M. I. Petrov, A. E. Krasnok, P. A. Belov, and Y. S. Kivshar, Phys. Rev. B **92**, 155415 (2015).
25. A. E. Krasnok, A. E. Miroshnichenko, P. A. Belov, and Y. S. Kivshar, Opt. Express **20**, 20599 (2012).
26. O. Merchiers, F. Moreno, F. González, and J. M. Saiz, Phys. Rev. A **76**, 043834 (2007).
27. A. B. Evlyukhin, C. Reinhardt, A. Seidel, B. S. Luk'yanchuk, and B. N. Chichkov, Phys. Rev. B **82**, 045404 (2010).
28. M. S. Wheeler, J. S. Aitchison, and M. Mojahedi, J. Opt. Soc. Am. B **27**, 1083 (2010).
29. R. A. Shore and A. D. Yaghjian, "Traveling electromagnetic waves on linear periodic arrays of small lossless penetrable spheres," Technical Report AFRL-SN-HS-TR-2004-044, DTIC Document (2004).
30. R. A. Shore and A. D. Yaghjian, Electron. Lett. **41**, 578 (2005).
31. R. A. Shore and A. D. Yaghjian, Radio Sci. **47**, RS2014 (2012).
32. L. Deych and A. Roslyak, Phys. Status Solidi C **2**, 3908 (2005).
33. L. I. Deych and O. Roslyak, Phys. Rev. E **73**, 036606 (2006).
34. C. Linton, V. Zalipaev, and I. Thompson, Wave Motion **50**, 29 (2013).
35. E. N. Bulgakov and A. F. Sadreev, Phys. Rev. A **92**, 023816 (2015).
36. R. F. Ndangali and S. V. Shabanov, J. Math. Phys. **51**, 102901 (2010).
37. C. W. Hsu, B. Zhen, J. Lee, S.-L. Chua, S. G. Johnson, J. D. Joannopoulos, and M. Soljacic, Nature **499**, 188 (2013).
38. E. N. Bulgakov and A. F. Sadreev, Phys. Rev. A **90**, 053801 (2014).
39. F. Monticone and A. Alù, Phys. Rev. Lett. **112**, 213903 (2014).
40. X. Gao, C. W. Hsu, B. Zhen, X. Lin, J. D. Joannopoulos, M. Soljačić, and H. Chen, "Formation mechanism of guided resonances and bound states in the continuum in photonic crystal slabs," ArXiv preprint arXiv:1603.02815 (2016).
41. S. G. Tikhodeev, A. L. Yablonskii, E. A. Muljarov, N. A. Gippius, and T. Ishihara, Phys. Rev. B **66**, 045102 (2002).
42. D. A. Bykov and L. L. Doskolovich, J. Lightwave Technol. **31**, 793 (2013).
43. R. A. Shore and A. D. Yaghjian, Radio Sci. **47**, RS2015 (2012).
44. J. A. Stratton, *Electromagnetic Theory* (McGraw-Hill, 1941).
45. S. Carrasco, B. E. A. Saleh, M. C. Teich, and J. T. Fourkas, J. Opt. Soc. Am. B **23**, 2134 (2006).
46. G. Vuye, S. Fisson, V. Nguyen Van, Y. Wang, J. Rivory, and F. Abelès, Thin Solid Films **233**, 166 (1993).
47. B. Zhen, C. W. Hsu, L. Lu, A. D. Stone, and M. Soljacic, Phys. Rev. Lett. **113**, 257401 (2014).